The Importance of the Shape of Cloud Droplet Size Distributions in Shallow Cumulus Clouds. Part II: Bulk Microphysics Simulations

ADELE L. IGEL AND SUSAN C. VAN DEN HEEVER

Colorado State University, Fort Collins, Colorado

(Manuscript received 23 December 2015, in final form 30 September 2016)

ABSTRACT

In this two-part study, relationships between the cloud gamma size distribution shape parameter, microphysical processes, and cloud characteristics of nonprecipitating shallow cumulus clouds are investigated using large-eddy simulations. In Part I, the dependence of the shape parameter (which is closely related to the distribution width) on cloud properties and processes was investigated. However, the distribution width also impacts cloud process rates and in turn cloud properties, and it is this aspect of the relationship that is explored in Part II and is discussed in the context of aerosol–cloud interactions. In simulations with a bulk microphysics scheme, it is found that the evaporation rates are much more sensitive to the value of the shape parameter than to the condensation rates. This is due to changes in both the rate of removal of mass and the rate of removal of fully evaporated droplets. As a result, cloud properties such as droplet number concentration, mean droplet diameter, and cloud fraction are strongly impacted by the value of the shape parameter, particularly in the subsaturated regions of the clouds. These changes can be on the same order of magnitude as changes due to increasing or decreasing the aerosol concentration by a factor of 16. Particular attention is paid to the impact of the shape parameter on cloud albedo. The cloud albedo increases as the shape parameter is increased as a result of the changes in evaporation. The magnitude of the increase is about 4 times larger than previous estimates. However, this increase in cloud albedo is largely offset by a decrease in the cloud fraction, which results in only small increases to the domain-average albedo. Implications for the aerosol relative dispersion effect are discussed.

1. Introduction

In Igel and van den Heever (2017, hereafter Part I), the sensitivity of the cloud droplet shape parameter ν to cloud processes and its dependence on cloud properties was explored in shallow cumulus clouds using large-eddy simulations employing bin microphysics schemes. Here in Part II, we run the same simulations, but with a bulk microphysics scheme that uses specified values of the shape parameter based on the bin microphysics scheme simulations in Part I, in order to investigate how the shape parameter in turn impacts condensation and evaporation rates, as well as the macrophysical and optical characteristics of the shallow cumulus clouds.

Example gamma size distributions with different shape parameters are shown in Fig. 1a. These distributions have the same total number and mass of cloud droplets. It can be seen that as the shape parameter increases, the distributions become relatively narrow. The cloud droplet shape parameter is closely related to a more general quantity called the relative dispersion ε ($\nu = 1/\varepsilon^2$), which is the ratio of the size distribution's standard deviation to its mean (e.g., Hsieh et al. 2009a). The value of the relative dispersion for each of the distributions in Fig. 1a is indicated in the legend.

There has been much discussion in the literature about how the cloud droplet relative dispersion impacts the optical properties of clouds. It has been shown that increasing the relative dispersion while keeping the mixing ratio and number concentration constant leads to a reduction in cloud albedo (Liu et al. 2008). Many past research simulations have assumed that the relative dispersion of the cloud droplet size distribution is constant. However, some observations, as well as theoretical arguments and parcel modeling of condensation, have indicated that the relative dispersion increases as aerosol and cloud droplet number concentrations increase (Martin et al. 1994; Costa et al. 2000; Liu and Daum 2002; Yum and Hudson 2005; Pawlowska et al. 2006; Liu et al. 2006; Peng et al. 2007; Pinsky et al. 2014). This increase in the relative dispersion results in an increase in the effective radius of the droplet size distribution (given a

Corresponding author e-mail: Adele L. Igel, aigel@ucdavis.edu

DOI: 10.1175/JAS-D-15-0383.1

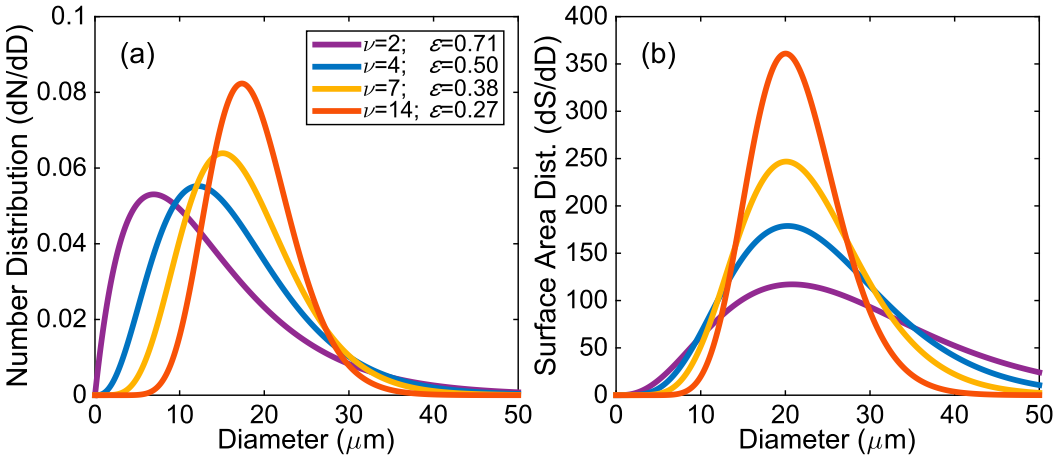

FIG. 1. Example gamma size distribution curves with different values of the shape parameter. The equivalent relative dispersion is also given in the legend. All curves have the same total number concentration and mixing ratio such that the mass mean diameter of all curves is 20 μm. (a) Droplet number distributions. The area under all curves (which is proportional to the total number concentration) is equal to 1. (b) The corresponding surface area (S) distributions.

constant droplet concentration and mass mixing ratio) and, hence, partially offsets the increase in cloud albedo associated with the increased aerosol and droplet concentrations. This has led to the term ''aerosol dispersion effect'' (e.g., Chen and Penner 2005).

It is not intuitively obvious that the distributions with a higher relative dispersion (lower shape parameter) in Fig. 1a have a larger effective radius since these distributions have both more small droplets and more large droplets. Recall that the effective radius is the ratio of the third moment (which is proportional to volume or mass) to the second moment (which is proportional to surface area) of the cloud droplet size distribution. The third moment of all distributions in Fig. 1a is the same since the total mass is assumed to be constant. The surface area distributions are shown in Fig. 1b. The total surface area is equal to the area under each curve. It is clear from Fig. 1b that the smallest droplets contribute little to the total surface area and that distributions with a higher relative dispersion have lower total surface area and hence a larger effective radius.

As discussed above, there is some observational evidence to support the relationship between the relative dispersion and the aerosol concentration. However, other observations compiled by Miles et al. (2000), observations from individual field campaigns (Zhao et al. 2006; Hsieh et al. 2009b; Geoffroy et al. 2010; Lu et al. 2007, 2008), and bin microphysics simulations of stratocumulus clouds (Part I; Lu and Seinfeld 2006) show a constant or decreasing relative dispersion with increasing droplet or aerosol concentration. Thus, it is unclear whether an aerosol dispersion effect exists.

Furthermore, most studies have not considered how a change to the relative dispersion or shape parameter of the cloud droplet size distribution will concomitantly impact cloud properties such as cloud fraction and mean droplet size. The results of Morrison and Grabowski (2007) suggest that switching from a low to a high shape parameter value results in a decrease of the effective radius and an increase in the cloud water path, droplet number concentration, and optical depth of shallow cumulus clouds. It seems then that we are still far from understanding the behavior of the relative dispersion of cloud droplet size distributions, and yet understanding this behavior could be important for enhancing our understanding of cloud processes and radiation on local as well as global scales (Peng and Lohmann 2003; Rotstayn and Liu 2003; Chen and Penner 2005).

In this study we will use simulations with a bulk microphysics scheme to first investigate the impact of the shape parameter on condensation and evaporation rates in nonprecipitating shallow cumulus clouds. We will then investigate how the changes in condensation and evaporation due to the chosen value of the shape parameter lead to further changes in the physical and optical properties of the clouds. Implications for the aerosol dispersion effect will be discussed. In addition, the relative sensitivity of the cloud properties to the shape parameter and to aerosol concentration will be assessed.

2. Methods

The same simulation setup that was used in Part I was also used here in Part II. The simulations using the Regional Atmospheric Modeling System (RAMS; Cotton et al. 2003) were designed to produce nonprecipitating shallow cumulus clouds and were initialized with semi-idealized conditions from Zhu and Albrecht (2003). The

TABLE 1. Summary of the two-moment bulk microphysics simulations.

Simulation	Description
BULK100-NU2, BULK100-NU4, BULK100-NU7, BULK100-NU14	Simulations using the RAMS double-moment bulk scheme (Saleeby and van den Heever 2013) using an initial aerosol concentration of 400 cm^{-3} and with a cloud droplet shape parameter value of 2, 4, 7, and 14, respectively.
BULK400-NU*x*, BULK1600-NU*x*	As above, but using aerosol concentrations of 100 and 1600 cm^{-3}, respectively. For each aerosol concentration, four simulations were run, one with each of the four cloud droplet shape parameter values (2, 4, 7, 14).
BULK400-NUe4-c7	As above, but with an initial aerosol concentration of 400 cm^{-3} in which a cloud droplet shape parameter value of 4 is used at subsaturated grid points, and a value of 7 is used at supersaturated grid points.

domain was 12.8 km × 12.8 km in horizontal extent with 50-m grid spacing and 3.5 km deep with 25-m grid spacing. Horizontal boundary conditions were periodic and a damping layer was placed in the top 500 m of the domain. A subgrid diffusion scheme was employed based on Smagorinsky (1963) with modifications by Lilly (1962) and Hill (1974). The simulations were run for 9.5 h. Clouds began to develop after about 4.5 h and only the 4 h of the simulation (hours 5.5–9.5) are used for analysis (for more information on the simulation design, see Part I).

Since there is disagreement in the literature about the relationship between the shape parameter and the aerosol concentration (see the introduction and Part I), we ran simulations with the RAMS bulk microphysics scheme (Saleeby and van den Heever 2013) in which the shape parameter and aerosol concentration were varied independently. Twelve simulations were run with the RAMS bulk microphysics scheme for the same three aerosol concentration values as in Part I (100, 400, and 1600 cm^{-3}) and for four cloud droplet shape parameter values (2, 4, 7, and 14). The values of 4 and 7 correspond to the approximate averages found in the sub- and supersaturated regions of the BIN simulations in Part I, and the values of 2 and 14 are the extreme average values reported in the literature for shallow cumulus clouds (Table 1 in Part I). It is important to note that in the RAMS bulk microphysics scheme, supersaturation is permitted to exist at the end of a time step and all condensation rates are calculated explicitly based on supersaturation and hydrometeor properties. A saturation adjustment scheme is not used. A shape parameter value of 2 was used for both the drizzle and rain hydrometeor categories, although the total amount of mass in these categories was minimal.

The simulations will be designated as BULK*x*-NU*y*, where *x* indicates the aerosol number concentration and *y* indicates the shape parameter value (e.g., BULK100-NU2 for the simulation with an aerosol concentration of 100 cm^{-3} and a cloud droplet shape parameter of 2). All simulations are listed in Table 1 for reference.

Aerosol particles are assumed to have a lognormal size distribution with a median radius of 40 nm and a spectral width of 1.8. They are depleted upon cloud droplet nucleation but are not regenerated upon cloud droplet evaporation. Constant entrainment of new aerosol particles into the continuously deepening boundary layer allows cloud droplet concentrations to remain approximately constant during the last 3 h of the simulation. Hydrometeors were radiatively active (Harrington 1997), but aerosol particles were not.

The cloud water path and column-integrated cloud droplet concentration of the cumulus clouds at the end of the simulations are shown in Fig. 2 for BULK400-NU2, BULK400-NU14, and BULK1600-NU2 in order to give the reader an idea of how the cumulus clouds in our simulations appear.

3. Shape parameter impact on condensation and evaporation rates

Having first looked at how cloud processes impact the shape parameter in Part I, we now want to investigate how the shape parameter impacts cloud characteristics through changes to microphysical process rates. Another motivation for conducting bulk microphysics scheme tests is to determine if the wide range of possible values based on observations (Table 1 in Part I; Miles et al. 2000) has a large impact on simulation results. The focus here is on the condensation and evaporation rates since those are the most dominant processes in the simulations of nonprecipitating shallow cumulus clouds. We will first examine the sensitivity of these processes to the shape parameter from a theoretical standpoint and then examine the sensitivity using the BULK simulations.

a. Theoretical perspective

1) CONDENSATION AND EVAPORATION OF CLOUD LIQUID WATER

It is useful to understand theoretically how the shape parameter is expected to impact the numerical simulations first in order to better interpret the differences in the simulated clouds. In these simulations of nonprecipitating

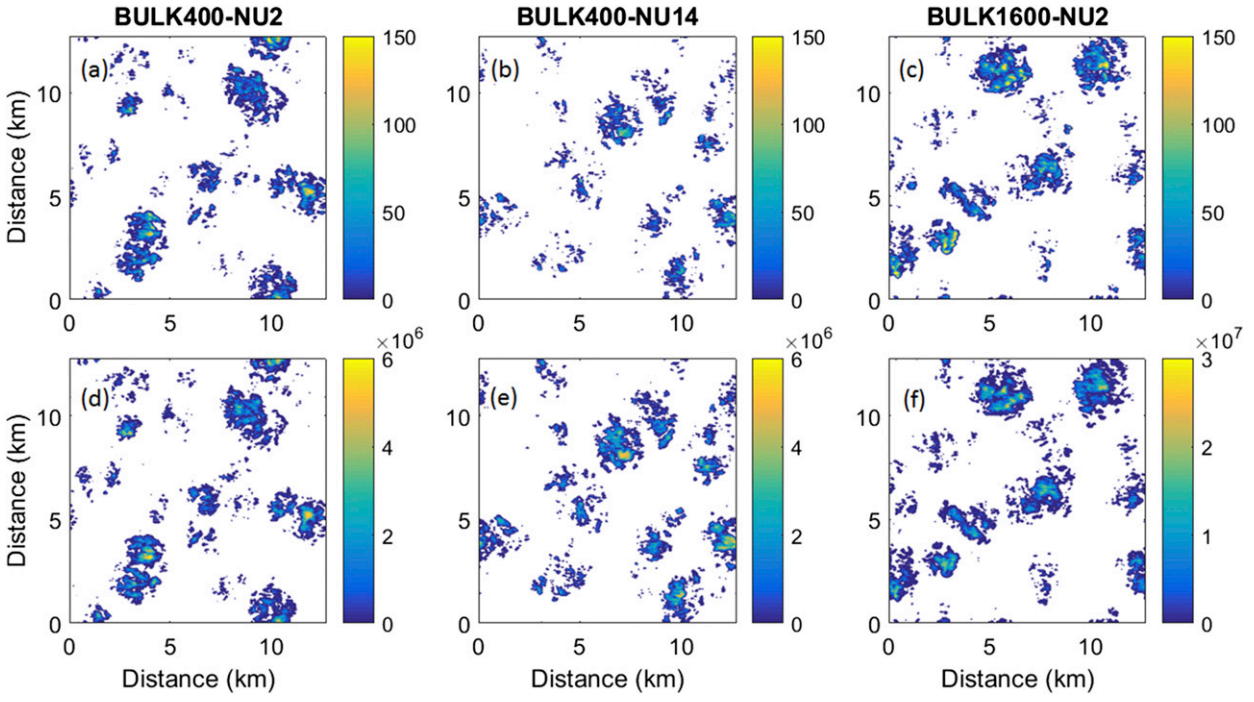

FIG. 2. (a)–(c) Liquid water path (g m^{-2}) and (d)–(f) column-integrated cloud droplet concentration (cm^{-2}) from (a),(d) BULK400-NU2, (b),(e) BULK400-NU14, and (c),(f) BULK1600-NU2 at the end of the simulations. The minimum liquid water path shown is 1 g m^{-2} and the minimum column-integrated cloud droplet concentration shown in 10^4 cm^{-2}.

cumulus clouds, the most important microphysical process is condensation/evaporation. By only looking at the gamma distributions provided in Fig. 1a, it is difficult to tell whether the condensation/evaporation rate of a droplet size distribution should increase or decrease for a higher shape parameter (lower relative dispersion). The condensation/evaporation rate of a single droplet is linearly proportional to its diameter. Distributions with a higher shape parameter have both fewer small and fewer large droplets but more medium-sized droplets, and thus it is difficult to predict how these changes in the size distribution will change the total condensation/evaporation rate. The condensation-/evaporation-rate ($\partial r_{c/e}/\partial t$) equation for a gamma distribution of cloud droplet sizes (neglecting the ventilation coefficient which is up to a 10% correction for cloud droplets) is related to the shape parameter in the following way:

$$\frac{\partial r_{c/e}}{\partial t} \propto \nu \left[\frac{\Gamma(\nu)}{\Gamma(\nu+3)}\right]^{1/3}. \qquad (1)$$

A full description of the condensation/evaporation equation used by the RAMS bulk microphysics scheme can be found in Walko et al. (2000). This relationship between the condensation rate and the shape parameter is shown in Fig. 3. It is evident from this figure that the condensation rate rapidly increases at low values of the shape parameter and more slowly approaches 1 as the value increases. There is a 35% increase in the total condensation rate from the low shape parameter value of 2 to the high value of 14 used in the simulations. Even the simulation with a shape parameter value of 4 can expect an increase of about 20% in the condensation rate if all else is equal (and the condensation rate is nonzero). Therefore, from a theoretical point of view, the

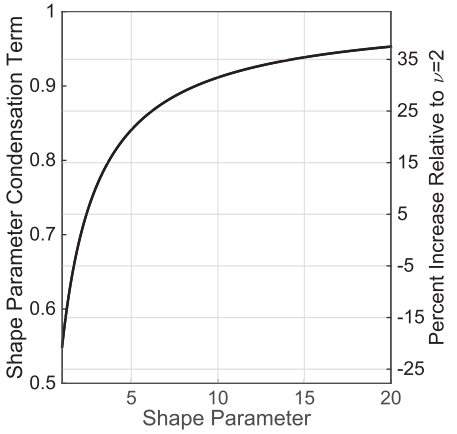

FIG. 3. Theoretical dependence of the condensation rate on the shape parameter. The left vertical axis shows the value of the shape parameter term [Eq. (1)] in the condensation equation, and the right vertical axis shows the percentage increase in the condensation rate from the condensation rate when the shape parameter equals 2.

shape parameter may be quite important for determining cloud growth rates and cloud droplet properties.

2) EVAPORATION OF CLOUD DROPLETS

In addition to impacting the condensation/evaporation rate, the shape parameter also influences how quickly droplets are fully evaporated. This rate will be referred to as the number evaporation rate. To avoid confusion, the evaporation of cloud droplet mass will henceforth be called mass evaporation. The change in number evaporation rate can best be explained by examining Fig. 1a. Gamma size distributions with the same mean mass diameter (same total mass and number of droplets) but with different shape parameters, such as those shown in Fig. 1a, have fewer small droplets as the shape parameter increases. Thus, gamma distributions with higher shape parameters will usually evaporate a lower fraction of the droplet number concentration in a given (short) time interval when all else is equal (unless all or nearly all droplets are evaporated). In other words, in some small time interval, these distributions will fully evaporate fewer droplets in the event of partial evaporation of the cloud mass. Note that this is not a result of any model parameterization—given a distribution of droplets characterized by a lower relative dispersion (higher shape parameter) in the real world, we would expect this same behavior. The resulting increase in the number of remaining droplets in a higher-shape-parameter case will feedback to and increase the mass evaporation rate in the subsequent time interval (since the mass evaporation rate is proportional to the droplet concentration) compared to a lower-shape-parameter case. It is straightforward to see that the mass evaporation rate should be proportional to the droplet concentration when considering the simple case of a monodisperse population of droplets—the mass evaporation rate in this case is the evaporation rate of an individual droplet multiplied by the total number of droplets.

To demonstrate this feedback between the mass and number evaporation rates, we ran the RAMS bulk microphysics evaporation routine offline. We initialized one grid point with $5\,\mathrm{g\,kg^{-1}}$ of cloud water and a cloud droplet concentration of $100\,\mathrm{cm^{-3}}$. Number and mass evaporation were the only processes allowed, and the relative humidity was kept fixed at 95%. All tests were run for 5 min with a 1-s time step. In the first set of tests (Figs. 4a–c), the shape parameter value used for both number and mass evaporation was set to 2, 4, 7, or 14. In the second set of tests (Figs. 4d–f), a shape parameter of 2 was always used in all tests for the number evaporation, while the mass evaporation again used values of 2, 4, 7, or 14. When the shape parameter is allowed to influence the number evaporation rate (Figs. 4a–c), there is a sharp decrease in the amount of time required for complete evaporation of the cloud water as the shape parameter is increased (Fig. 4a; 6.8 min for $\nu = 2$ and 1.4 min for $\nu = 14$). A decrease in the time required for mass evaporation is also seen in the tests where the shape parameter is only varied for the mass evaporation rate (Fig. 4d; 6.8 min for $\nu = 2$ and 5.2 min for $\nu = 14$) as we would expect based on Eq. (1) and Fig. 3, but the decrease is not nearly so large as in the case where the shape parameter is varied for both number and mass evaporation. The much faster mass evaporation of the cloud water (Figs. 4a,c) for higher shape parameters (when the shape parameter impacts the number evaporation rate) is due to the fact that the number concentration of droplets remains high (Fig. 4b). Since the mass evaporation rate is proportional to the number concentration, a higher number concentration will promote higher mass evaporation rates. Similar results were found by Pinsky et al. (2016), who used a parcel model with bin microphysics to show that an initially narrow cloud droplet distribution evaporates more mass more quickly than an initially wide cloud droplet distribution.

To show that this behavior is not specific to the RAMS bulk microphysics scheme, we performed analogous offline experiments using the evaporation routine from the Hebrew University bin scheme (Khain et al. 2004). This bin scheme is the same as the one used in Part I of the study. The experiments using this bin scheme were initialized using the same conditions as for the bulk experiments shown in Figs. 4a–f. The bulk scheme evaporation experiments, which rely on a constant shape parameter, cannot be exactly repeated with a bin scheme since the bin scheme will allow the shape and width of the droplet size distribution to change with time. So, to make the bin scheme behave like a bulk scheme, the droplet size distributions were reinitialized after each time step with the predicted mixing ratio and number concentration such that they conformed to a gamma distribution with the specified shape parameter. The results of these experiments, referred to as "bin as bulk," for $\nu = 2$ and $\nu = 14$ are shown in the solid lines in Figs. 4g–i. To reproduce the experiments in Figs. 4d–f (where different values of the shape parameter are used for the mass and number evaporation) with the bin scheme, a similar procedure was used except that the cloud mixing ratio was predicted with a droplet size distribution that was reinitialized using the shape parameter specified for mass evaporation, and the droplet concentration was predicted with a droplet size distribution that was reinitialized with a shape parameter of 2. The result for $\nu = 14$ is shown in the dashed line in Figs. 4g–i ("bin as bulk test"; the result is the same as the solid line for the corresponding $\nu = 2$ experiment). By comparing these results to the bulk evaporation results, it is easily seen that the two schemes produce the same qualitative dependence on the shape parameter.

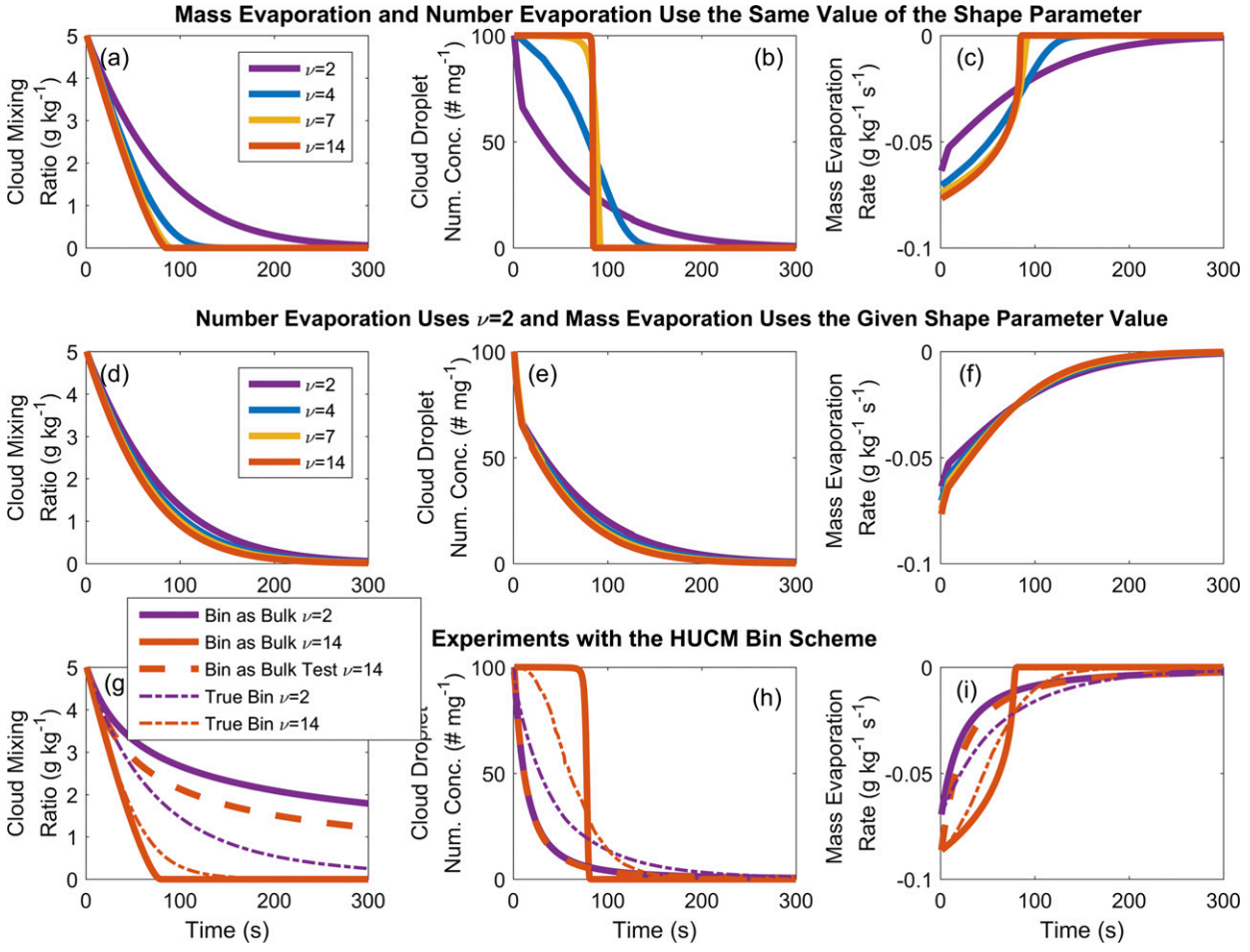

FIG. 4. Evolution of (a),(d) cloud mixing ratio, (b),(e) cloud droplet number concentration, and (c),(f) mass evaporation rate for two different experiments with the bulk microphysics scheme stand-alone evaporation routines. In (a)–(c), the specified value of the shape parameter is used for both number and mass evaporation. In (d)–(f), the specified value of the shape parameter is used only for the mass evaporation, and the number evaporation uses a shape parameter value of 2. (g)–(i) Experiments analogous to (a)–(c) are shown with solid lines (but using the bin scheme), an experiment analogous to (d)–(f) is shown with the dashed line, and the true bin scheme experiments are shown with the thin dashed–dotted lines. See the text for more details.

Finally, we also ran the bin scheme without any reinitialization of the droplet size distributions; in other words, we ran the bin scheme as an actual bin scheme (''true bin'' in the thin dashed–dotted lines in Figs. 4g–i). While the evolution of the cloud water mixing ratio and droplet number concentration in these two experiments are not nearly as dissimilar as the case of the $\nu = 2$ and $\nu = 14$ bulk scheme experiments (Figs. 4a,b), the qualitative behavior is nonetheless similar. For both schemes, the initially narrow distribution ($\nu = 14$) is slower to fully evaporate droplets at the beginning but, ultimately, is able to evaporate all of the cloud water much sooner than the initially wide distribution ($\nu = 2$). Again, these results are consistent with similar experiments conducted by Pinsky et al. (2016).

This theoretical analysis of the condensation and mass and number evaporation rates cannot account for the more complicated feedbacks that will occur in real clouds, nor how actual condensation rates over a finite time step will be limited by the supersaturation since the supersaturation is often quite low. To investigate whether these sensitivities of the condensation/mass evaporation and number evaporation rates to the shape parameter exist in clouds, we now look at the BULK simulations of nonprecipitating shallow cumulus clouds.

b. *BULK simulations*

1) CONDENSATION AND EVAPORATION RATES

For simplicity, the impact of the shape parameter on condensation and mass evaporation rates is investigated

in the BULK400 simulations only. Similar results are found with the BULK100 and BULK1600 simulations. All cloudy points (grid points that are defined to be cloudy if they contain 0.01 g kg^{-1} of cloud water or more) in these simulations were grouped into 1% relative humidity bins. For each relative humidity bin, the average condensation or mass evaporation rate was calculated and is shown in Fig. 5a. In agreement with the theoretical concepts discussed in section 3a, the condensation and mass evaporation rates increase in magnitude as the shape parameter increases. However, the percentage increase in the condensation and mass evaporation rates (Fig. 5b) are much higher than predicted by Eq. (1) and Fig. 3. For instance, in the condensation regime the BULK400-NU14 condensation rates for RH between 101% and 104% are about 60% higher than the BULK400-NU2 condensation rates (Fig. 5b). For mass evaporation rates, the increase (more negative values) is particularly large; the percentage increase of NU14 relative to NU2 approaches 600% (Fig. 5b). The greater sensitivity of the mass evaporation rates to the shape parameter compared to the sensitivity of the condensation rates to the shape parameter is consistent with the tests shown in Fig. 4, which demonstrate that feedbacks between the number and mass evaporation rates enhance the rate at which cloud water is evaporated. Similar tests to those in Fig. 4 (in which the shape parameter was only allowed to vary for the mass evaporation rate) but for the shallow cumulus clouds confirm that it is the feedbacks with the number evaporation rate that enhance the sensitivity of the mass evaporation rates (not shown).

While only the BULK400 simulations have been examined here, the same behavior is seen in the BULK100 and BULK1600 simulations. Similar analysis but using the BIN simulations from Part I are also qualitatively similar (not shown) and suggest that the results found here are not unique to the RAMS bulk microphysics scheme; rather they are more general and help to elucidate the microphysical processes and feedbacks that occur in real clouds.

2) Mixing between saturated and unsaturated cloudy air

A fifth sensitivity test, designated BULK400-NUe4-c7, in which the shape parameter is set to 4 where cloud is evaporating and to 7 where cloud is condensing, was run to investigate the relative importance of the shape parameter in supersaturated and subsaturated regions of the clouds. Figures 5a and 5b show that the average mass evaporation rate in the BULK400-NUe4-c7 test is essentially identical to that in the BULK400-NU4 test. This may not be too surprising given that in both simulations the shape parameter used for all evaporation calculations is 4. However, this result indicates that the changed shape parameter in the supersaturated regions (which is set to 7 in BULK400-NUe4-c7) has little impact in the subsaturated regions of the cloud. On the other hand, the value of the shape parameter in the subsaturated regions does appear to affect the condensation rates. The condensation rates in the BULK400-NUe4-c7 test lie between the condensation rates for the NU4 and NU7 tests (Fig. 5b). Therefore, although the condensation rates in the BULK400-NUe4-c7 test are enhanced relative to the BULK400-NU4 test, they are still heavily influenced by the value of the shape parameter in the subsaturated regions of the cloud, presumably as a result of mixing between the saturated and subsaturated air.

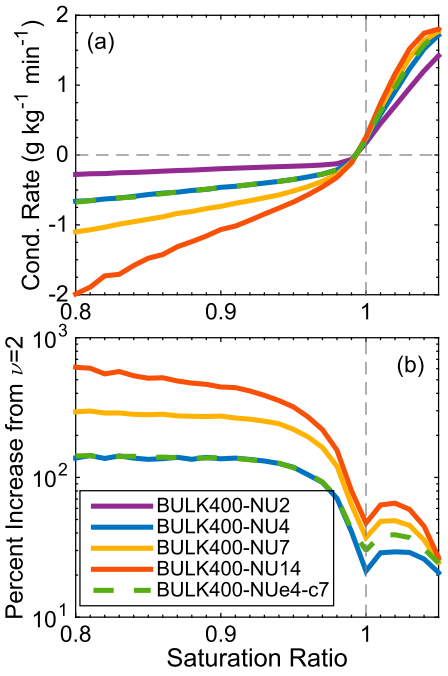

FIG. 5. For the BULK400 simulations, (a) the condensation rate as a function of saturation ratio and (b) the percentage increase of the condensation rate relative to the condensation rate in BULK400-NU2. Note that the green dashed line in both panels often lies on top of the blue line. See the text for further details.

4. Shape parameter impacts on cloud properties

a. *Macroscopic cloud characteristics*

Now we will focus on how the changes to the condensation and mass evaporation rates found in section 3 impact the macrophysical properties of the clouds. As we saw in the previous section, there are large differences in the condensation and mass evaporation rates as a function of relative humidity when the shape parameter is varied; however, these differences may or

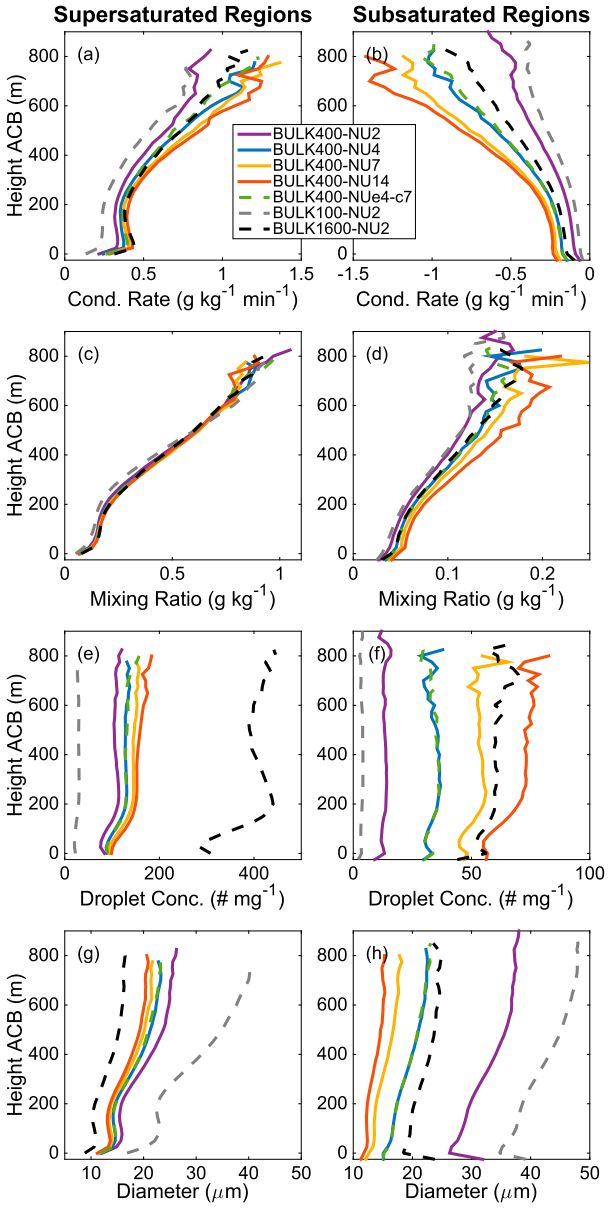

FIG. 6. Average vertical profiles of (a),(b) condensation rate, (c),(d) cloud mixing ratio, (e),(f) cloud droplet concentration, and (g),(h) mean cloud diameter in (a),(c),(e),(g) supersaturated regions and (b),(d),(f),(h) subsaturated regions of the clouds from the BULK400-NUx simulations as a function of height above cloud base (ACB).

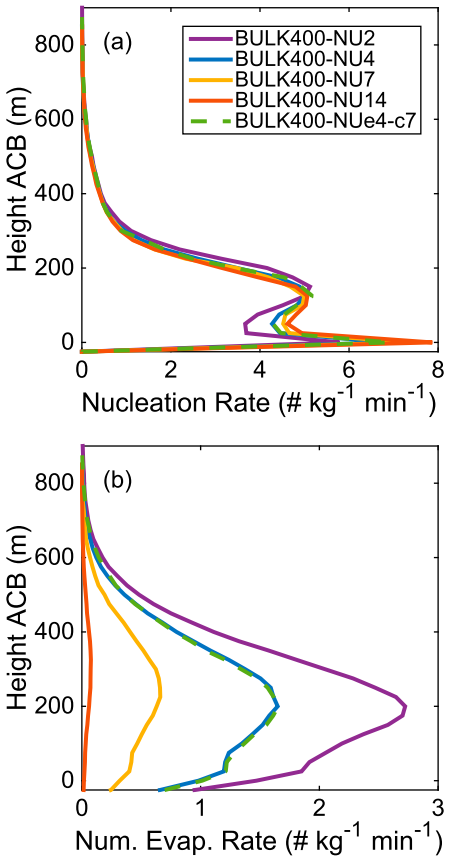

FIG. 7. Time- and domain-averaged vertical profiles ACB of (a) the cloud droplet nucleation rate and (b) the cloud droplet number evaporation rate from the BULK400-NUx simulations.

may not have a significant impact on the macroscopic features of the shallow clouds being simulated here.

To investigate whether these changes are important for the cloud field as a whole, we plot vertical profiles of selected quantities from some of the BULK simulations in Figs. 6 and 7. Since the boundary layer depth and cloud-base height is increasing in time, creating average vertical profiles of clouds to facilitate comparisons is not trivial. Here, we have used image-processing techniques to identify individual clouds. A grid box is considered cloudy if the cloud water mixing ratio is greater than 0.01 g kg^{-1}, and cloudy grid boxes are defined to be connected using a six-connected neighborhood; in other words, cloudy grid boxes must share a full face with its neighbor in order to be connected. For each cloud, cloud base is defined as the first vertical level above the surface that is saturated or supersaturated. All clouds are aligned relative to cloud base, and then mean vertical profiles are calculated.

Figures 6a and 6b show that the cloud-averaged condensation and mass evaporation rates do in fact increase as the shape parameter increases, just as we expect based on the results from section 3. Nonetheless, because of the strong mixing between saturated and unsaturated regions of these cumulus clouds, and because the increased condensation and mass evaporation rates tend to offset one another, the average cloud water mixing ratio is nearly identical in all of the BULK simulations in the saturated zones (Fig. 6c). In the subsaturated regions of the cloud, the mixing ratio is

somewhat increased for the higher shape parameter tests (Fig. 6d) despite the fact that the higher shape parameter tests have higher mass evaporation rates (Fig. 6b). The reason for these increased mixing ratios lies in changes to the frequency of cloud mixing ratio values in the subsaturated zone (not shown). In the BULK400-NU2 test, mass evaporation rates are slow and there are many points with very low cloud mixing ratios. In contrast, in the BULK400-NU14 test, mass evaporation rates are fast and there are far fewer points with very low mixing ratios. As a result of this shift in the frequency of cloudy points in the subsaturated region as the value of the shape parameter is varied, the average value of the cloud water mixing ratio is highest in the BULK400-NU14 test, despite the fact that the mass evaporation rate in this test is also highest.

Although the cloud water contents are similar across all shape parameter tests, the cloud droplet number concentration is quite different across these tests in both the saturated and subsaturated zones; there are about 50 cm^{-3} more droplets (~400% increase for the subsaturated region) in the BULK400-NU14 test than in the BULK400-NU2 test in both regions (Figs. 6e,f). Since the cloud water mixing ratio is similar in all simulations, the change in number concentration results in a change to the average cloud droplet diameter—there is a decrease in the average diameter in supersaturated regions of about 5 μm (Fig. 6g) and in the subsaturated regions of about 20 μm (Fig. 6h) when going from the BULK400-NU14 test to the BULK400-NU2 test.

The changes in number concentration in the saturated zone cannot be explained by changes in the number of droplets nucleated (Fig. 7a). Instead, these changes are attributed to the impact of the shape parameter on the number evaporation rate (Fig. 7b) and the strong mixing that exists between saturated and unsaturated regions. Whereas the changes in mass evaporation and condensation rates could approximately offset one another, there is no mechanism to offset the decrease in the number evaporation rate (Fig. 7b) in the subsaturated regions caused by an increase in the shape parameter (see section 2 for more discussion of the number evaporation rate). However, recall that aerosol regeneration upon cloud droplet evaporation is not turned on in these simulations. If it had been represented, the mixing of regenerated aerosol particles back into the supersaturated regions of the cumulus clouds, and the subsequent activation of these particles may have been able to partially offset some of the changes we see to the number concentration of droplets in the supersaturated regions (Fig. 6e). The importance of the role of regenerated aerosols should be addressed in a future study.

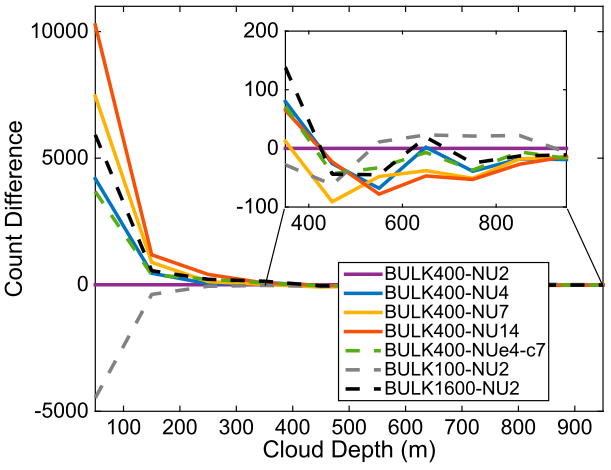

FIG. 8. The difference relative to the BULK400-NU2 simulation in the number of simulated clouds as a function of cloud depth. The inset shows a zoomed-in portion of the plot.

b. *Cloud sizes and cloud fraction*

Images of the cloud field at the end of the BULK400-NU2 and BULK400-NU14 simulations are shown in Fig. 2. The BULK400-NU14 simulation appears to have more small clouds than the BULK400-NU2 simulation. Associated with these changes is the appearance of a lower cloud fraction in the BULK400-NU14 simulation. We will now investigate these changes to the cloud fields more quantitatively.

As discussed above, image-processing techniques were used to identify individual clouds in the simulations. For each cloud, the cloud depth was calculated as the distance from cloud base to the highest cloudy point in the cloud. The cloud depths were binned using intervals of 100 m. Cloud frequency counts, expressed as a difference from those in the BULK400-NU2 simulation, are shown in Fig. 8. It is evident from this figure that as the shape parameter increases, there is an increase in the number of the shallowest clouds and a decrease in the number of all deeper clouds. While the fact that the condensation rate and associated latent heating increases as the shape parameter increases (Figs. 5 and 6a) might suggest that clouds with a higher shape parameter would be more buoyant and deeper, the deeper clouds do not occur. Instead, it appears that the larger mass evaporation rates that are also associated with an increased shape parameter (Fig. 6b) result in more rapid evaporation of the cloud top as dry air is entrained and hence ultimately shallower clouds.

Associated with the shift to shallower clouds in the high-shape-parameter BULK simulations is a shift to lower cloud fractions (Fig. 9c). Here, the cloud fraction has been calculated by counting the number of cloudy

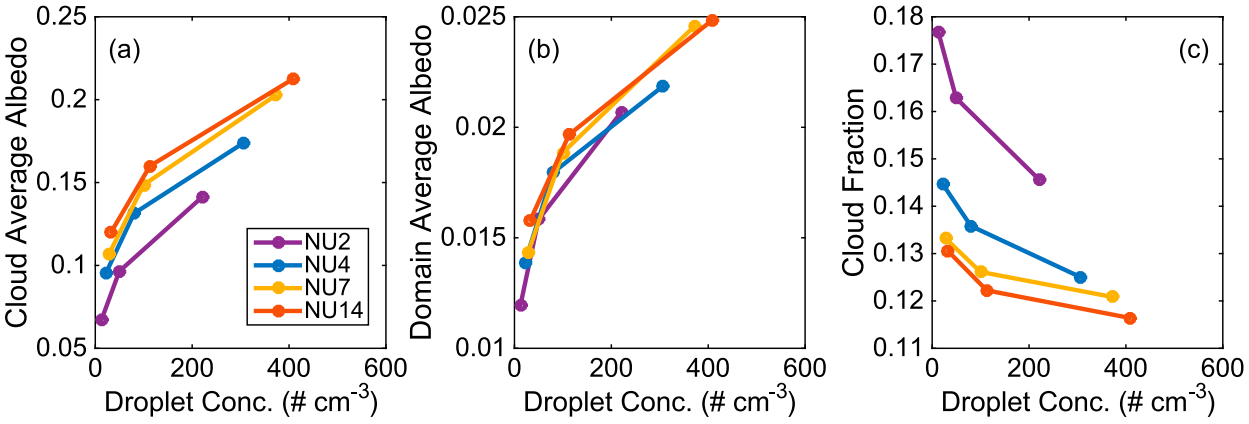

FIG. 9. (a) Cloud-average albedo, (b) domain-average albedo where a value of 0 is used when there is no cloud, and (c) cloud fraction plotted as a function of the cloud-average droplet concentration for all of the BULK simulations. Leftmost points along each line are from the BULK100 simulations, middle points are from the BULK400 simulations, and rightmost points are from the BULK1600 simulations.

columns (where a cloudy column is defined as any column with at least one grid point that has a cloud mixing ratio greater than 0.01 g kg^{-1}) and dividing by the total number of columns. Again, even though the higher-shape-parameter simulations have more total clouds than the lower-shape-parameter simulations (Fig. 8), the faster mass evaporation associated with high shape parameters results in faster evaporation of cloud edges and hence a lower cloud fraction.

Finally, BULK400-NUe4-c7, which uses a shape parameter value of 4 for evaporation and a value of 7 for condensation, more closely resembles the BULK400-NU4 test than the BULK400-NU7 test in every quantity shown in Figs. 6–8. This same result was found in the detailed condensation and evaporation analysis (Fig. 5). These results have important implications for choosing an appropriate shape parameter in simulations that use a constant value for this parameter. Specifically, it is more important to correctly represent the size distribution characteristics of the evaporating part of the cloud than it is the condensing part of the cloud. Incorrect choices in this regard will impact many cloud properties, including cloud height, cloud fraction, and droplet concentration, as have been discussed above.

While we have only shown the sensitivity of the macroscopic cloud properties to the shape parameter from the BULK400 tests, the same qualitative results were seen in the BULK100 and BULK1600 simulations as well but are not shown here.

c. *Relative importance of the shape parameter and aerosol concentration*

In Figs. 6 and 8, the results of BULK100-NU2 and BULK1600-NU2 are also shown in order to assess how the sensitivity of cloud properties to changes in the shape parameter compares to the sensitivity of cloud properties to a 16-fold increase in the aerosol concentration. For some cloud properties, such as the droplet number concentration and mean mass diameter in supersaturated regions (Figs. 6e and 6g), the change in aerosol concentration results in a much larger response than does the change in the shape parameter. This is probably not surprising given that the droplet concentration is the field most directly impacted by the aerosol concentration. For other fields—namely, the mean condensation rate (Fig. 6a), the mean mixing ratio in supersaturated regions (Fig. 6c), the droplet number concentration and size in subsaturated regions (Figs. 6f and 6h), and the cloud depth frequency (Fig. 8)—the range of responses is of about the same magnitude for both the aerosol concentration tests and the shape parameter tests. However, for some fields, particularly those most closely related to the evaporation rate (Figs. 6b and 6d), the sensitivity to the shape parameter is larger than it is to the aerosol concentration. These relative magnitudes of response are summarized in Table 2.

If there is in fact a systematic relationship between the aerosol concentration and the mean shape parameter or relative dispersion of the cloud droplet distribution, the large impact of the shape parameter on some cloud properties could have important implications for understanding aerosol–cloud interactions. For example, consider the cloud fraction shown in Fig. 9c. For a constant shape parameter (any line in Fig. 9c), the cloud fraction always decreases as the aerosol concentration (mean droplet concentration) increases. However, if the shape parameter should decrease as the aerosol concentration increases, as has been suggested by some (e.g., Martin et al. 1994; Costa et al. 2000; Liu and Daum 2002), then the cloud fraction may

TABLE 2. Summary of the relative magnitude of response to aerosol concentration and to cloud droplet shape parameter of the quantities shown in Figs. 6, 8, and 9c. The C indicates supersaturated regions of the clouds (where droplets grow by condensation), and the E indicates subsaturated regions of the clouds (where droplets are evaporating).

	Response to aerosol concentration is larger	Responses are about equal	Response to shape parameter is larger
Condensation rate		×	
Evaporation rate			×
Cloud mixing ratio (C)		×	
Cloud mixing ratio (E)			×
Droplet number concentration (C)	×		
Droplet number concentration (E)		×	
Droplet diameter (C)	×		
Droplet diameter (E)		×	
Cloud depth frequency		×	
Cloud fraction			×

instead actually increase with increasing aerosol concentration according to Fig. 9c. More specifically, in Fig. 9c the cloud fraction for low droplet concentration and high shape parameter (leftmost orange point) is lower than that for high droplet concentration and low shape parameter (rightmost purple point). Thus, the shape parameter may be an important parameter in the context of aerosol–cloud interactions.

d. *Cloud optical properties*

Finally, we will investigate how the shape parameter impacts the optical properties of clouds. Our simulations have shown that increasing the relative dispersion (decreasing the shape parameter) increases the mean droplet diameter and decreases the number of droplets in cumulus clouds while keeping the cloud water content nearly constant, particularly in the supersaturated regions of the cloud (Fig. 6). This increase in the mean droplet diameter and decrease in the number concentration will further reduce the cloud albedo and radiative forcing for clouds with higher relative dispersion, and hence the relative dispersion of cloud droplets may be more important than previously thought for determining cloud radiative characteristics.

The cloud albedo for these simulations were calculated from the cloud mixing ratio r and number concentration N using the same formulas as in Liu et al. (2008) and assuming the same value of the asymmetry parameter of 0.85 for consistency. The cloud albedo is a function of the cloud effective radius r_e, which is given by the following equation:

$$r_e = \frac{(\nu+2)^{2/3}}{[\nu(\nu+1)]^{1/3}}\left(\frac{3r}{4\pi\rho_w N}\right)^{1/3}. \quad (2)$$

The average albedo of cloudy columns is shown in Fig. 9a, where again a cloudy column is defined as a column with at least one grid point that has a cloud mixing ratio greater than 0.01 g kg^{-1}. Consistent with Liu et al. (2008), the albedo increases as the shape parameter increases, but the magnitude of the increase is larger than that predicted by Liu et al. (2008). For example, the increase is about 0.06 between the BULK100-NU2 and BULK100-NU14 simulations, which is greater than the 0.015 increase predicted by Liu et al. (2008).

As discussed above, there are two factors that drive the increase in albedo with shape parameter. There is a "direct" factor discussed by Liu et al. (2008) in which, if all else is equal, a higher shape parameter corresponds to a lower effective radius and, hence, a higher albedo. This is the response that is obtained by varying ν in Eq. (2) but holding r and N constant. There is also an "indirect" factor, which is the impact of the shape parameter on changes to the microphysical properties of clouds, specifically the number of cloud droplets and their size. Likewise, this is the response that is obtained by keeping ν constant in Eq. (2) but allowing r and N to vary. (These direct and indirect factors are not to be confused with direct and indirect aerosol effects.) To determine which factor is more important, the cloud-average albedo is recalculated for the simulations in two different ways.

1) Calculate the magnitude of the direct factor: The cloud albedo is calculated offline for each of the NU2 simulations (BULK100-NU2, BULK400-NU2, and BULK1600-NU2), once with each of the four values (2, 4, 7, and 14) of the shape parameter tested in this study where that value appears in Eq. (2), but always with the cloud number concentration and cloud mixing ratio predicted by the appropriate NU2 simulation. In other words, for calculating the effective radius, ν is allowed to vary but r and N are not allowed to vary and specifically always utilize the values from the appropriate NU2 simulation.
2) Calculate the magnitude of the indirect factor: The cloud-average albedo for each simulation is calculated offline using the cloud properties predicted by each simulation, but using a shape parameter value of 2 where that value appears in Eq. (2). In other words, for calculating the effective radius that is used by the albedo equation, ν is always set equal to 2, but r and N are allowed to vary and utilize the values predicted by each of the simulations.

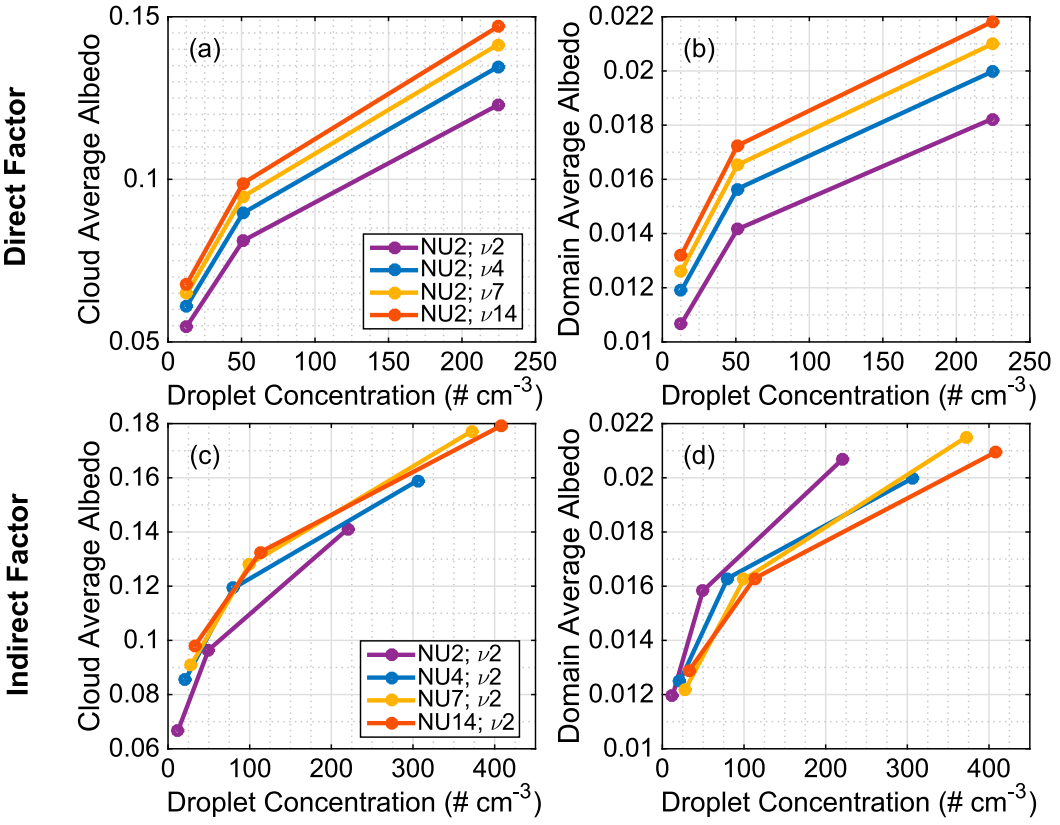

FIG. 10. (a),(c) Cloud-average albedo and (b),(d) domain-average cloud albedo calculated from the BULK simulations. In (a) and (b) all albedo calculations use the NU2 simulations for cloud properties and the indicated value of the shape parameter (ν in the legend) in order to assess the direct factor, and in (c) and (d) all albedo calculations use the indicated simulations for cloud properties but use a shape parameter value of 2 in order to assess the indirect factor. See the text for more details.

The results of these calculations are shown in Fig. 10. The increase in cloud albedo as the shape parameter increases owing to the direct factor ranges from about 0.01 to 0.025 for a given droplet concentration (Fig. 10a). The magnitude of the indirect factor is more difficult to estimate for a given droplet concentration since all simulations have different mean droplet concentrations; however, the increase in cloud albedo as the shape parameter increases owing to the indirect factor is likely to be about 0.03 (Fig. 10c). These two factors added together approximate the total change in albedo (through a Taylor expansion of the albedo equation). These results indicate that the indirect factor can amplify the total change in albedo by a factor of about 2–4 (from about 0.025 to 0.055 in the BULK1600 simulations and from about 0.01 to about 0.04 in the BULK100 simulations). Thus, it is important to consider both the direct and indirect factors when determining the impact of the relative dispersion on cloud albedo.

The domain-average albedo (Fig. 9b) is more important than the cloud-average albedo from a climate perspective. It can be seen in Fig. 9b than the domain-average albedo increases as the shape parameter increases but is less sensitive to the shape parameter than is the cloud-average albedo (Fig. 9a). Although the cloud-average albedo increases with the shape parameter, as discussed above, the cloud fraction decreases as this parameter increases by up to 7% in the cleanest simulations (Fig. 9c). These two changes compete with one another in terms of the domain-average albedo and, as a result, the domain-average albedo is approximately constant (Fig. 9b). Nonetheless, the domain-average albedo still increases as the shape parameter increases. This change in the domain-average albedo can again be attributed to both direct and indirect factors (Fig. 10), where the indirect factor (factor due to changes in the number concentration and mass mixing ratio) is influenced by both the change in cloud fraction and the change in cloud microphysical properties (the latter being the only contributor to the indirect factor for cloud-average albedo). It is evident that the direct change to domain-average albedo (Fig. 10b; magnitude is about 0.002–0.003) is larger than the indirect

change to this quantity (Fig. 10d; magnitude is at most 0.001). The indirect change to the domain-average albedo is small since the decrease in cloud fraction offsets most of the increase in albedo associated with the change in microphysical properties. For the shallow cloud regime, a change in albedo of 0.001 from the indirect factor is small and can likely be neglected, but at higher cloud fractions, should the same feedback processes be active, the indirect factor may become much larger and be required for accurate representation of cloud albedo.

e. *Implications for the relative dispersion effect*

The aerosol relative dispersion effect states that if the shape parameter (relative dispersion) decreases (increases) as the droplet concentration increases, then the increase in cloud albedo associated with an increase in the droplet concentration will be partially offset by the change in shape of the droplet distribution. For example, in Fig. 10a or 10b, moving from the leftmost orange point to the rightmost purple point (i.e., increasing droplet concentration and decreasing shape parameter) results in a smaller change in albedo than does moving from the leftmost orange point to the rightmost orange point (i.e., increasing droplet concentration without changing the shape parameter).

However, to our knowledge, previous studies have not considered how the shape parameter will simultaneously impact the cloud properties as has been done here. In terms of cloud-average albedo, Figs. 9 and 10 suggest that the relative dispersion effect will be larger than previously thought. However, in terms of domain-average albedo, Figs. 9 and 10 suggest that the changes in cloud-average albedo and cloud fraction will mostly offset one another, in which case accounting for the indirect impact of the shape parameter on domain-average albedo is not important.

That being said, it is seen that the cloud fraction becomes less sensitive to the shape parameter as the droplet concentration increases (Fig. 9c; bigger spread among leftmost points than rightmost points on each line). Consequently, the importance of the shape parameter for the domain-average albedo may be a function of the cloud fraction or even cloud type. It is difficult to ascertain from these simulations whether this is in fact the case since the average droplet concentrations are so different in each of the BULK1600 simulations (Fig. 9). More simulations are needed in the future in order to address these questions.

5. Conclusions

In the second part of this two-part study, simulations of nonprecipitating shallow cumulus clouds have been conducted using the RAMS double-moment bulk microphysics scheme. With these simulations, several issues pertaining to the relationships between the cloud droplet distribution relative dispersion, aerosol concentration, and cloud properties have been investigated.

The simulations with the RAMS bulk microphysics scheme have provided insight into the importance of the shape parameter for condensation and evaporation. They indicated that the average mass evaporation rate can increase fivefold or more for a given RH value as the shape parameter is increased from 2 to 14. Increases in the average condensation rate were also seen but were not as large. The primary pathway for these enhancements to the condensation and mass evaporation rates was through changes to the number of fully evaporated drops. It is believed that this result is not specific to the particular microphysics scheme used in this study, since the same results were seen when using a bin scheme. Furthermore, the feedbacks between the droplet number and mass evaporation rates were seen to operate when the evaporation scheme was run offline with no impacts from any other processes. Thus, we speculate that this feedback is not unique to shallow cumulus clouds and should operate in all cloud types.

An additional simulation with the RAMS bulk microphysics scheme was used to test the importance of the spatial variability of the shape parameter in which the shape parameter was set to 4 during evaporation and to 7 during condensation. These values were chosen based on results from the BIN simulations in Part I. This simulation revealed that the value of the shape parameter for condensation had almost no influence on the mass evaporation rates, whereas the value of the shape parameter for mass and number evaporation did influence the condensation rates. This is good news for numerical modelers. It suggests that only the shape parameter in subsaturated regions of the cloud needs to be appropriately specified and that perhaps it may not be necessary to represent the spatial variability of the shape parameter in simulations of shallow nonprecipitating cumulus clouds.

These impacts of the shape parameter on condensation and evaporation had consequences for the macroscopic properties of the clouds. Varying the shape parameter was found to result in only small changes to the cloud mixing ratio, but substantial (in terms of percentage increase) changes to the droplet concentration and mean diameter of cloud droplets, particularly in the subsaturated regions of clouds. The changes in the subsaturated region of the cloud due to changes in the shape parameter were sometimes larger than the changes resulting from differences in the initial aerosol concentration.

Finally, we investigated the impact of the chosen shape parameter value on cloud optical properties. We found that increasing the shape parameter led to increases in the

cloud-average albedo as a result of both changes in the number and size of droplets and to changes in the droplet distribution shape itself. This increase in the cloud albedo was about 4 times larger than would be expected if no changes to the number and size of droplets had been simulated. However, the increased cloud albedo was mostly offset by a decrease in the cloud fraction due to higher evaporation rates, which resulted in little sensitivity of the domain-average albedo to the shape parameter. Should the aerosol relative dispersion effect exist, we did not find that accounting for shape-parameter-induced changes to the cloud properties and cloud fraction would greatly impact the magnitude of this effect.

The results discussed here can only be applied to nonprecipitating, shallow continental cumulus clouds. However, we can speculate about how precipitation might impact these results. A higher shape parameter suppresses autoconversion (e.g., Seifert and Beheng 2001), which would lead to higher droplet number concentrations for higher shape parameters. Here, we have shown how higher shape parameters lead to higher droplet number concentrations as a result of changes in evaporation. Thus, it might be expected that precipitation processes would enhance some of the sensitivities seen here rather than mute them. More work is needed to understand the impacts of the shape parameter and similar studies looking at other cloud types should be conducted.

Acknowledgments. The authors thank three anonymous reviewers for providing helpful comments that led to improvements to this paper. This material is based on work supported by the National Science Foundation Graduate Research Fellowship Program under Grant DGE-1321845 and the National Aeronautics and Space Administration Grant NNX13AQ32G.

REFERENCES

Chen, Y., and J. E. Penner, 2005: Uncertainty analysis for estimates of the first indirect aerosol effect. *Atmos. Chem. Phys.*, **5**, 2935–2948, doi:10.5194/acp-5-2935-2005.

Costa, A. A., C. J. de Oliveira, J. C. P. de Oliveira, and A. J. da Costa Sampaio, 2000: Microphysical observations of warm cumulus clouds in Ceará, Brazil. *Atmos. Res.*, **54**, 167–199, doi:10.1016/S0169-8095(00)00045-4.

Cotton, W. R., and Coauthors, 2003: RAMS 2001: Current status and future directions. *Meteor. Atmos. Phys.*, **82**, 5–29, doi:10.1007/s00703-001-0584-9.

Geoffroy, O., J.-L. Brenguier, and F. Burnet, 2010: Parametric representation of the cloud droplet spectra for LES warm bulk microphysical schemes. *Atmos. Chem. Phys.*, **10**, 4835–4848, doi:10.5194/acp-10-4835-2010.

Harrington, J. Y., 1997: *The Effects of Radiative and Microphysical Processes on Simulation of Warm and Transition Season Arctic Stratus.* Colorado State University, 289 pp.

Hill, G. E., 1974: Factors controlling the size and spacing of cumulus clouds as revealed by numerical experiments. *J. Atmos. Sci.*, **31**, 646–673, doi:10.1175/1520-0469(1974)031<0646:FCTSAS>2.0.CO;2.

Hsieh, W. C., H. Jonsson, L.-P. Wang, G. Buzorius, R. C. Flagan, J. H. Seinfeld, and A. Nenes, 2009a: On the representation of droplet coalescence and autoconversion: Evaluation using ambient cloud droplet size distributions. *J. Geophys. Res.*, **114**, D07201, doi:10.1029/2008JD010502.

——, A. Nenes, R. C. Flagan, J. H. Seinfeld, G. Buzorius, and H. Jonsson, 2009b: Parameterization of cloud droplet size distributions: Comparison with parcel models and observations. *J. Geophys. Res.*, **114**, D11205, doi:10.1029/2008JD011387.

Igel, A. L., and S. C. van den Heever, 2017: The importance of the shape of cloud droplet size distributions in shallow cumulus clouds. Part I: Bin microphysics simulations. *J. Atmos. Sci.*, **74**, 249–258, doi:10.1175/JAS-D-15-0382.1.

Khain, A., A. Pokrovsky, M. Pinsky, A. Seifert, and V. Phillips, 2004: Simulation of effects of atmospheric aerosols on deep turbulent convective clouds using a spectral microphysics mixed-phase cumulus cloud model. Part I: Model description and possible applications. *J. Atmos. Sci.*, **61**, 2963–2982, doi:10.1175/JAS-3350.1.

Lilly, D. K., 1962: On the numerical simulation of buoyant convection. *Tellus*, **14**, 148–172, doi:10.1111/j.2153-3490.1962.tb00128.x.

Liu, Y., and P. H. Daum, 2002: Anthropogenic aerosols: Indirect warming effect from dispersion forcing. *Nature*, **419**, 580–581, doi:10.1038/419580a.

——, ——, and S. S. Yum, 2006: Analytical expression for the relative dispersion of the cloud droplet size distribution. *Geophys. Res. Lett.*, **33**, L02810, doi:10.1029/2005GL024052.

——, ——, H. Guo, and Y. Peng, 2008: Dispersion bias, dispersion effect, and the aerosol–cloud conundrum. *Environ. Res. Lett.*, **3**, 045021, doi:10.1088/1748-9326/3/4/045021.

Lu, M.-L., and J. H. Seinfeld, 2006: Effect of aerosol number concentration on cloud droplet dispersion: A large-eddy simulation study and implications for aerosol indirect forcing. *J. Geophys. Res.*, **111**, D02207, doi:10.1029/2005JD006419.

——, W. C. Conant, H. H. Jonsson, V. Varutbangkul, R. C. Flagan, and J. H. Seinfeld, 2007: The Marine Stratus/Stratocumulus Experiment (MASE): Aerosol-cloud relationships in marine stratocumulus. *J. Geophys. Res.*, **112**, D10209, doi:10.1029/2006JD007985.

——, G. Feingold, H. H. Jonsson, P. Y. Chuang, H. Gates, R. C. Flagan, and J. H. Seinfeld, 2008: Aerosol-cloud relationships in continental shallow cumulus. *J. Geophys. Res.*, **113**, D15201, doi:10.1029/2007JD009354.

Martin, G. M., D. W. Johnson, and A. Spice, 1994: The measurement and parameterization of effective radius of droplets in warm stratocumulus clouds. *J. Atmos. Sci.*, **51**, 1823–1842, doi:10.1175/1520-0469(1994)051<1823:TMAPOE>2.0.CO;2.

Miles, N. L., J. Verlinde, and E. E. Clothiaux, 2000: Cloud droplet size distributions in low-level stratiform clouds. *J. Atmos. Sci.*, **57**, 295–311, doi:10.1175/1520-0469(2000)057<0295:CDSDIL>2.0.CO;2.

Morrison, H., and W. W. Grabowski, 2007: Comparison of bulk and bin warm-rain microphysics models using a kinematic framework. *J. Atmos. Sci.*, **64**, 2839–2861, doi:10.1175/JAS3980.

Pawlowska, H., W. W. Grabowski, and J.-L. Brenguier, 2006: Observations of the width of cloud droplet spectra in stratocumulus. *Geophys. Res. Lett.*, **33**, L19810, doi:10.1029/2006GL026841.

Peng, Y., and U. Lohmann, 2003: Sensitivity study of the spectral dispersion of the cloud droplet size distribution on the indirect aerosol effect. *Geophys. Res. Lett.*, **30**, 1507, doi:10.1029/2003GL017192.

——, ——, R. Leaitch, and M. Kulmala, 2007: An investigation into the aerosol dispersion effect through the activation process in marine stratus clouds. *J. Geophys. Res.*, **112**, D11117, doi:10.1029/2006JD007401.

Pinsky, M., I. P. Mazin, A. Korolev, and A. Khain, 2014: Supersaturation and diffusional droplet growth in liquid clouds: Polydisperse spectra. *J. Geophys. Res. Atmos.*, **119**, 12 872–12 887, doi:10.1002/2014JD021885.

——, A. Khain, A. Korolev, and L. Magaritz-Ronen, 2016: Theoretical investigation of mixing in warm clouds—Part 2: Homogeneous mixing. *Atmos. Chem. Phys.*, **16**, 9255–9272, doi:10.5194/acp-16-9255-2016.

Rotstayn, L. D., and Y. Liu, 2003: Sensitivity of the first indirect aerosol effect to an increase of cloud droplet spectral dispersion with droplet number concentration. *J. Climate*, **16**, 3476–3481, doi:10.1175/1520-0442(2003)016<3476:SOTFIA>2.0.CO;2.

Saleeby, S. M., and S. C. van den Heever, 2013: Developments in the CSU-RAMS aerosol model: Emissions, nucleation, regeneration, deposition, and radiation. *J. Appl. Meteor. Climatol.*, **52**, 2601–2622, doi:10.1175/JAMC-D-12-0312.1.

Seifert, A., and K. D. Beheng, 2001: A double-moment parameterization for simulating autoconversion, accretion and selfcollection. *Atmos. Res.*, **59–60**, 265–281, doi:10.1016/S0169-8095(01)00126-0.

Smagorinsky, J., 1963: General circulation experiments with the primitive equations. *Mon. Wea. Rev.*, **91**, 99–164, doi:10.1175/1520-0493(1963)091<0099:GCEWTP>2.3.CO;2.

Walko, R. L., W. R. Cotton, G. Feingold, and B. Stevens, 2000: Efficient computation of vapor and heat diffusion between hydrometeors in a numerical model. *Atmos. Res.*, **53**, 171–183, doi:10.1016/S0169-8095(99)00044-7.

Yum, S. S., and J. G. Hudson, 2005: Adiabatic predictions and observations of cloud droplet spectral broadness. *Atmos. Res.*, **73**, 203–223, doi:10.1016/j.atmosres.2004.10.006.

Zhao, C., and Coauthors, 2006: Aircraft measurements of cloud droplet spectral dispersion and implications for indirect aerosol radiative forcing. *Geophys. Res. Lett.*, **33**, L16809, doi:10.1029/2006GL026653.

Zhu, P., and B. Albrecht, 2003: Large eddy simulations of continental shallow cumulus convection. *J. Geophys. Res.*, **108**, 4453, doi:10.1029/2002JD003119.